

Article

Origin of the Size-Dependent Stokes Shift in CsPbBr₃ Perovskite Nanocrystals

Michael Christopher Brennan, John Herr, Triet S. Nguyen-Beck, Jessica Zinna, Sergiu Draguta, Sergei Rouvimov, John Parkhill, and Masaru Kuno

J. Am. Chem. Soc., **Just Accepted Manuscript** • DOI: 10.1021/jacs.7b05683 • Publication Date (Web): 03 Aug 2017

Downloaded from <http://pubs.acs.org> on August 3, 2017

Just Accepted

“Just Accepted” manuscripts have been peer-reviewed and accepted for publication. They are posted online prior to technical editing, formatting for publication and author proofing. The American Chemical Society provides “Just Accepted” as a free service to the research community to expedite the dissemination of scientific material as soon as possible after acceptance. “Just Accepted” manuscripts appear in full in PDF format accompanied by an HTML abstract. “Just Accepted” manuscripts have been fully peer reviewed, but should not be considered the official version of record. They are accessible to all readers and citable by the Digital Object Identifier (DOI®). “Just Accepted” is an optional service offered to authors. Therefore, the “Just Accepted” Web site may not include all articles that will be published in the journal. After a manuscript is technically edited and formatted, it will be removed from the “Just Accepted” Web site and published as an ASAP article. Note that technical editing may introduce minor changes to the manuscript text and/or graphics which could affect content, and all legal disclaimers and ethical guidelines that apply to the journal pertain. ACS cannot be held responsible for errors or consequences arising from the use of information contained in these “Just Accepted” manuscripts.

Origin of the Size-Dependent Stokes Shift in CsPbBr₃ Perovskite Nanocrystals

Michael C. Brennan,[†] John E. Herr,[†] Triet S. Nguyen-Beck,[†] Jessica Zinna,[†]
Sergiu Draguta,[†] Sergei Rouvimov,[‡] John Parkhill*,[†] and Masaru Kuno*,[†]

[†]*Department of Chemistry and Biochemistry, University of Notre Dame*

251 Nieuwland Science Hall, Notre Dame, Indiana 46556, USA

[‡]*Notre Dame Integrated Imaging Facility, University of Notre Dame, Notre Dame, Indiana
46556, USA*

E-mail: mkuno@nd.edu, john.parkhill@nd.edu

Abstract

The origin of the size-dependent Stokes shift in CsPbBr₃ nanocrystals (NCs) is explained for the first time. Stokes shifts range from 82 to 20 meV for NCs with effective edge lengths varying from ~4 to 13 nm. We show that the Stokes shift is intrinsic to the NC electronic structure and does not arise from extrinsic effects such as residual ensemble size distributions, impurities or solvent-related effects. The origin of the Stokes shift is elucidated via first-principles calculations. Corresponding theoretical modeling of the CsPbBr₃ NC density of states and band structure reveal the existence of an intrinsic confined hole state 260 to 70 meV above the valence band edge state for NCs with edge lengths from ~2 to 5 nm. A size-dependent Stokes shift is therefore predicted and is in quantitative agreement with the experimental data. Comparison between bulk and NC calculations show that the confined hole state is exclusive to NCs. At a broader level, the distinction between absorbing and emitting states in

CsPbBr₃ is likely a general feature of other halide perovskite NCs and can be tuned via NC size to enhance applications involving these materials.

Introduction

Hybrid lead halide perovskites have been successfully implemented as effective, low-cost light absorbers in photovoltaic devices.¹ Within the relatively short period of time since their rediscovery,^{2,3} light-to-electricity conversion efficiencies have exceeded 20%.⁴ This success has stimulated tremendous interest in using hybrid perovskites, such as methylammonium lead iodide (MAPbI₃, MA=CH₃NH₃⁺), for solar cells and for a host of other applications.⁵ The remarkable properties of bulk lead halide perovskites have motivated research into harnessing the intrinsic size and compositional control over the optical/electrical response of corresponding nanostructured hybrid perovskites.⁶

Recent breakthroughs in colloidal chemistry now permit MAPbX₃, FAPbX₃ [FA = CH(NH₂)₂⁺; X = I⁻, Br⁻, Cl⁻] and their all-inorganic counterparts (CsPbX₃) to be made as high quality colloidal nanocrystals (NCs),⁷⁻⁹ nanowires,¹⁰⁻¹² and nanosheets.¹³⁻¹⁶ These nanomaterials are especially attractive materials for next generation lighting and display technologies due to their high photoluminescence (PL) quantum yields (QY ~40–90%), narrow emission linewidths (70–140 meV), and size-/composition-tunable band gaps.⁷⁻⁹ Despite reports that now exist on their electronic structure,¹⁷⁻¹⁹ much less is known about their underlying photophysics and the nature of the emitting state.

In particular, ubiquitous Stokes shifts (ΔE_s) exist in hybrid^{8,13,20} and all-inorganic lead halide perovskite nanostructures^{7,11,13,16,21-24} as well as in their thin-film counterparts.^{15,25} For CsPbBr₃ NCs, the Stokes shift is size-dependent and ranges from 82 to 20 meV for particles with effective edge lengths (l) between ~4 and 13 nm, respectively. This suggests that a distinction exists between absorbing and emitting states. Although recent studies have discussed the spectral properties and excited state dynamics of CsPbBr₃ NCs,^{20,23,26-29}

1
2
3 the origin of their size-dependent Stokes shift has yet to be explained.
4

5 As a historical note, analogous size-dependent Stokes shifts were observed two decades
6 ago in colloidal CdSe quantum dots (QDs). Stokes shifts there likewise ranged from ~ 100 to
7 10 meV for particle diameters between ~ 1 and 5 nm.³⁰ Corresponding research³¹ ultimately
8 explained this shift, yielding a more in-depth understanding about the electronic structure
9 of CdSe QDs, which are today an important model system.^{32,33} A similar elucidation of
10 the origin of the Stokes shift in CsPbBr₃ NCs will improve our understanding about the
11 photophysics of this new system and will ultimately be crucial in promoting their eventual
12 use within applications.
13
14
15
16
17
18
19
20
21

22 In a recent study, we have demonstrated that a size-dependent Stokes shift exists in
23 CsPbBr₃ NCs.³⁴ Here we establish that it is not caused by extrinsic factors and rationalize
24 its origin using detailed theoretical calculations of the size-dependent density of states (DOS)
25 and electronic structure of CsPbBr₃ NCs. These computational results reveal the existence
26 of an inherent, size-dependent, confined hole state 260 to 70 meV above the valence band
27 edge state for particles with sizes between ~ 2 and 5 nm. We also show that the confined
28 hole state is robust across NC size and crystal phase. We propose that this state is relatively
29 dark in absorption due to its low DOS, but bright in emission. This, in turn, explains the
30 experimentally-observed size-dependent Stokes shift. We further illustrate that the emit-
31 ting state possesses low cesium character, likely providing insight into the PL properties of
32 analogous nanostructured lead halide perovskites (e.g. MAPbX₃).
33
34
35
36
37
38
39
40
41
42
43
44
45

46 Results and Discussion

47
48
49 Nineteen CsPbBr₃ NC ensembles were synthesized using the technique described by Prote-
50 sescu et al.⁷ Resulting NCs adopt cuboidal morphologies and have surfaces passivated
51 with oleylammonium and oleate ligands.³⁵ **Figure 1** shows representative low- and high-
52 magnification TEM images of four ensembles, which span the size series. The low-magnification
53
54
55
56
57
58
59
60

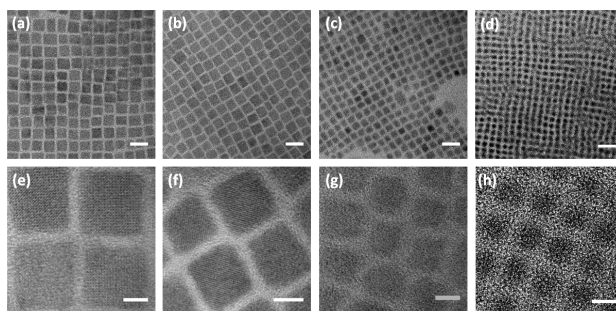


Figure 1: Representative low- [(a) $l = 12.8$ nm, (b) $l = 8.5$ nm, (c) $l = 6.8$ nm, (d) $l = 4.2$ nm] and high- [(e) $l = 12.8$ nm, (f) $l = 8.5$ nm, (g) $l = 6.8$ nm, (h) $l = 4.1$ nm] magnification TEM images of CsPbBr₃ NCs. Scale bars on low- and high-magnification images are 20 and 5 nm, respectively.

micrographs show that the NCs form close packed areas with residual size distributions in the range of 5–20%. **Figure S1** illustrates sizing histograms from where effective edge lengths and size distributions have been obtained. **Figure S2** illustrates an experimental sizing curve extracted from the data. Powder X-ray diffraction (PXRD) patterns shown in **Figure S3** confirm the crystallinity of the NCs. Both TEM and PXRD data, in turn, suggest that the NCs predominately adopt a cubic crystal structure, although it should be noted that there is considerable debate^{36–38} in the literature as to the actual lattice adopted by these NCs.

Size-dependent Stokes Shift

Figure 2a now shows ensemble absorption and emission spectra from seven representative samples (corresponding edge lengths from ~ 4 to 13 nm). NCs are dispersed in toluene and emission is induced using an excitation energy far above the band edge ($E_{exc} = 3.543$ eV; $\lambda_{exc} = 350$ nm). Excitation intensities are low ($I_{exc} \sim 1.4 \mu\text{W}/\text{cm}^2$) and are within the linear (single exciton) regime. Additional details regarding this can be found in **Figure S4**. The data reveal that, as l decreases, both band edge absorption and emission energies blueshift. This has been explained as stemming from quantum confinement effects given a CsPbBr₃ bulk exciton Bohr radius of $a_0 = 3.5$ nm.⁷ Apart from the structured absorption, the high

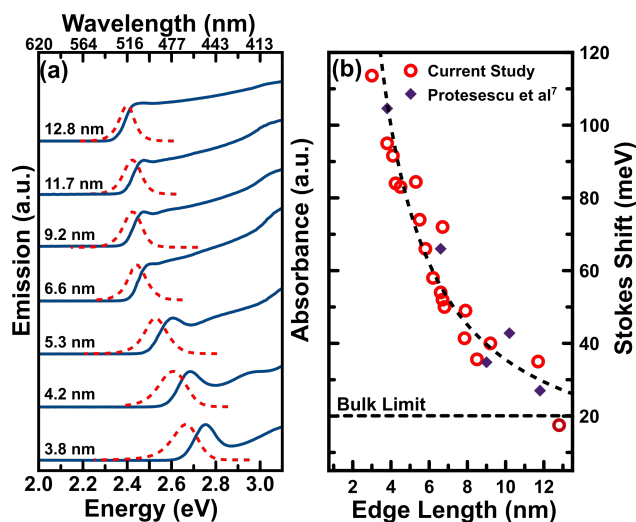


Figure 2: (a) Ensemble absorption (solid blue lines) and emission (dashed red lines) spectra from a small size series of CsPbBr₃ NCs dispersed in toluene. Above gap excitation ($E_{exc} = 3.543$ eV, $\lambda_{exc} = 350$ nm) used to acquire PL spectra. All absorption/emission spectral pairs offset for clarity. (b) Corresponding size-dependent Stokes shifts and those extracted from existing literature.⁷

quality of the as-produced NCs is evident from measured PL quantum yields, which range from 30 to 60% along with narrow emission line widths between 90 and 170 meV (Tables S1 and S2 respectively).

The most notable observation in Figure 2a is the apparent Stokes shift between the band edge absorption and emission in each case. This Stokes shift decreases with increasing edge length as quantified by fitting acquired ensemble absorption/emission data. Representative absorption fits and extracted data are shown in Figure S5 and Table S2 of the SI. What emerges is a size-dependent Stokes shift (ΔE_s) that ranges from 115 to 17 meV as the effective edge length decreases from ~ 3 to 13 nm. Figure 2b summarizes these shifts and contains additional data points extracted from the literature.⁷ Note that the bulk Stokes shift is roughly 20 meV³⁹ as is indicated by the dashed horizontal line in Figure 2b.

Room-temperature PL excitation (PLE) measurements confirm the size dependence of ΔE_s . Namely, Figures 3a,b show representative spectra for $l = 8.5$ nm (Figure 3a) and $l = 4.2$ nm (Figure 3b) ensembles. In each case, PLE spectra have been acquired by monitoring the red edge of each sample's band edge emission. Monitored energies are denoted

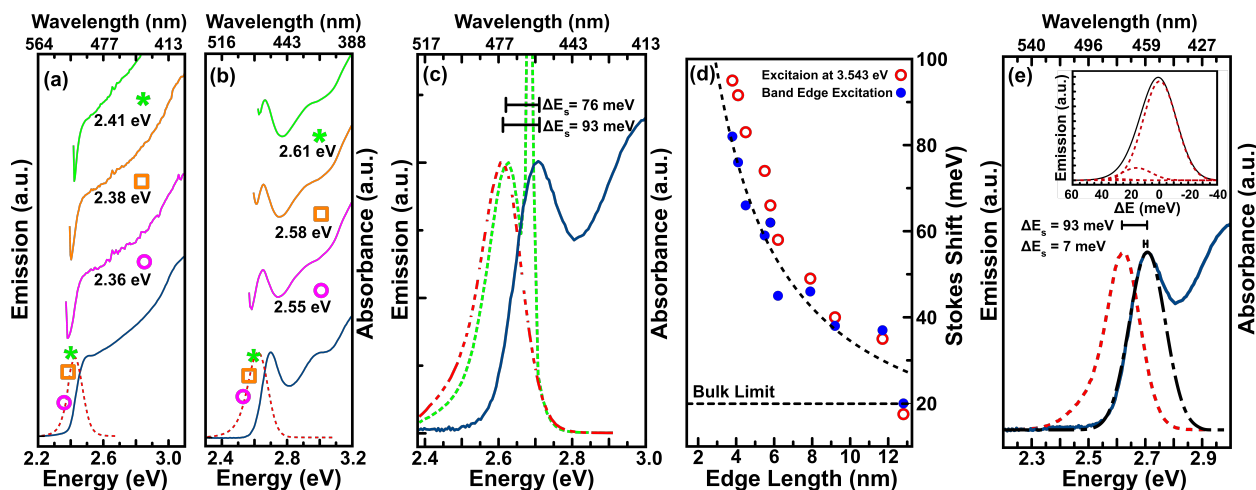


Figure 3: PLE spectra acquired on (a) $l = 8.5$ nm and (b) $l = 4.2$ nm NC ensembles at three energies on the red edge of their above gap excitation-derived emission spectra. (c) PL spectra of a $l = 4.1$ nm sample recorded using band edge ($\lambda_{exc} = 460$ nm, dashed green line) and above gap ($\lambda_{exc} = 350$ nm, dashed-dotted red line) excitation energies. Corresponding absorption is given in solid blue. Extracted Stokes shifts (ΔE_s) provided at the top right. (d) ΔE_s vs. edge length of $l = 3.8, 4.1, 4.5, 5.5, 5.8, 6.2, 7.9, 9.2, 11.7,$ and 12.8 nm ensembles using both band edge (closed blue circles) and above gap ($E_{exc} = 3.543$ eV, open red circles) excitation. The dashed line is a fit to band edge excitation-acquired ΔE_s values. (e) Results of the convolution analysis (dashed-dotted line) for the $l = 4.1$ nm ensemble. Associated absorption and emission spectra are shown as solid blue and dashed red lines, respectively. Inset: Modeled single particle spectrum with a Huang-Rhys parameter of $S = 0.11$.

with colored symbols. Resulting PLE spectra match corresponding linear absorption spectra. The correlation is especially evident in the 4.2 nm ensemble where the room temperature band edge excitonic feature is clearly resolved. Corresponding average PLE-derived Stokes shifts are ~ 77 and 34 meV for the $l = 4.2$ and 8.5 nm ensembles respectively. Of note is that these PLE-derived shifts are slightly smaller than corresponding values seen in **Figure 2b**. This likely stems from the residual size distribution of each ensemble given that the PLE measurement selectively monitors the largest NCs present.

To further verify the existence of a Stokes shift, we eliminate other possible extrinsic origins. First, we examine the time evolution of the emission maximum through time-correlated single photon counting time-resolved emission spectroscopy (TCSPC-TRES). Measurements were performed on $l = 4.1$ and 7.9 nm NC ensembles in toluene. These TCSPC-TRES results, shown in **Figure S6**, display negligible (≤ 5 meV) redshifting of the emission maximum over

1
2
3 the course of 4 ns following excitation. This suggests that solvatochromism or other effects
4
5 with slow degrees of freedom do not contribute to the apparent absorption/emission shift.
6

7 To establish that the Stokes shift is independent of dielectric media, we have addition-
8 ally recorded absorption/emission spectra in hexane and chloroform. Resulting Stokes shifts
9 quantitatively agree with values in **Figure 2b** and deviate by no more than 10 meV across
10 solvents. This is illustrated in **Figure S7a**, which plots Stokes shift data from CsPbBr₃
11 ($\epsilon_{\infty} = 4.96$)⁷ NC ensembles dispersed in hexane, toluene, and chloroform (associated static
12 dielectric constants: $\epsilon_{\text{hex}} = 1.88$, $\epsilon_{\text{tol}} = 2.38$, and $\epsilon_{\text{chlo}} = 4.81$).⁴⁰ The only observed solvent-
13 dependent effect is a blueshift of absorption/emission spectra in toluene and chloroform rela-
14 tive to that in hexane. This is summarized in **Figure S7b**, which shows absorption/emission
15 spectra of a $l = 4.2$ nm ensemble in the same three solvents. The effect likely stems from
16 dielectric contrast wherein increasing (decreasing) the permittivity difference between NCs
17 and their surrounding medium increases (decreases) exciton binding energies and results in
18 corresponding spectral redshifts (blueshifts).⁴¹
19
20
21
22
23
24
25
26
27
28
29
30
31

32 Next, we quantify contributions of the residual size distribution to ΔE_s , something first
33 suggested by earlier PLE measurements (**Figures 3a,b**). This is done by exciting samples
34 at their respective band edge and comparing observed Stokes shifts to those obtained when
35 exciting further to the blue. Motivating this is the fact that larger NCs in an ensemble absorb
36 more strongly at large energies because of their sizable density of states.⁴² Consequently, the
37 emission of an above gap excited NC ensemble possesses an enhanced contribution from
38 larger NCs in the distribution.⁴³
39
40
41
42
43
44
45

46 **Figure 3c** shows results of this measurement for a $l = 4.1$ nm ensemble excited at its
47 band edge ($E_{\text{exc}} = 2.696$ eV, $\lambda_{\text{exc}} = 460$ nm) and further to the blue at $E_{\text{exc}} = 3.543$ eV
48 ($\lambda_{\text{exc}} = 350$ nm). Evident is a decrease of the measured Stokes shift from $\Delta E_s = 93$ meV to
49 76 meV when exciting at the band edge. This clearly shows that the residual ensemble size
50 distribution influences observed Stokes shifts. Of added note, the extracted $\Delta E_s = 76$ meV
51 shift is in excellent agreement with the earlier PLE-derived $\Delta E_s = 77$ meV Stokes shift for
52
53
54
55
56
57
58
59
60

1
2
3 a $l = 4.2$ nm ensemble.
4

5 As a consequence, **Figure 3d** plots band edge excitation-derived ΔE_s values against l
6 for 10 NC ensembles. Observed Stokes shifts (filled blue circles) range from 82 to 20 meV
7 for l -values between 3.8 and 12.8 nm. Associated shifts, obtained when exciting further to
8 the blue at $E_{exc} = 3.543$ eV are also provided using open red circles. In all cases, differences
9 between band edge and above gap excitation Stokes shifts are apparent. These differences
10 decrease with increasing l from ~ 15 meV at $l \leq 7.0$ nm to ≤ 5 meV at $l \geq 7.0$ nm. As
11 added note, exciting samples progressively to the red, beyond their respective band edges,
12 causes monotonic decreases in observed ΔE_s , as expected from **Figure 3d**. Representative
13 absorption/emission spectra from samples excited at the band edge are provided in **Figure**
14 **S8**. The data in **Figure 3d** thus indicates that actual size-dependent ΔE_s values in CsPbBr₃
15 NCs range from 82 to 20 meV for $l = 3.8$ – 12.8 nm. A corresponding emission-based sizing
16 curve is provided in the *SI*.
17
18
19
20
21
22
23
24
25
26
27
28
29

30 As added verification of size distribution effects on ΔE_s , we model the Stokes shift by
31 convoluting a theoretical single particle emission spectrum with a Gaussian function repre-
32 sentative of the residual size distribution.³¹ The Gaussian takes a ~ 90 – 140 meV linewidth
33 and is established through fits to the band edge linear absorption. The single particle spec-
34 trum consists of a thermally broadened phonon progression and uses a literature longitudinal
35 optical (LO) phonon energy of $\omega_{LO} = 16$ meV^{44–46} as well as a Huang-Rhys parameter (S)
36 that takes values between $S = 0.11$ ⁴⁵ and $S = 0.45$.⁴⁶ The inset in **Figure 3e** illustrates the
37 employed single particle spectrum for the case where $S = 0.11$.
38
39
40
41
42
43
44
45

46 **Figure 3e** plots the resulting theoretical emission spectrum (dashed-dotted line, $S =$
47 0.11 , 140 meV linewidth) for a $l = 4.1$ nm sample relative to corresponding experimental
48 absorption and emission spectra. An apparent Stokes shift of 7 meV is evident. For $S = 0.45$,
49 ΔE_s increases to 9 meV. These shifts, in turn, agree with ΔE_s differences seen in **Figures**
50 **3c,d** for samples excited at the band edge and above gap. More importantly, the modeled
51 Stokes shift differs significantly from the experimentally-determined ΔE_s value of 76 meV
52
53
54
55
56
57
58
59
60

1
2
3
4
5
6
7
8
9
10
11
12
13
14
15
16
17
18
19
20
21
22
23
24
25
26
27
28
29
30
31
32
33
34
35
36
37
38
39
40
41
42
43
44
45
46
47
48
49
50
51
52
53
54
55
56
57
58
59
60

($E_{exc} = 2.696$ eV). Analogous results have been obtained for $l = 5.3$ nm and $l = 11.7$ nm ensembles (**Figure S9**). In all cases, modeled Stokes shifts are less than 10 meV enabling us to conclude that while residual NC size distributions influence observed Stokes shifts they do not account for either their origin or size dependence.

Theoretical Models

Having evidenced that the size-dependent Stokes shift in CsPbBr₃ NCs is not explained by extrinsic factors, we now focus on rationalizing an intrinsic origin by employing first-principles calculations. This requires a description of the electronic structure of CsPbBr₃. **Figures 4a,b** show the calculated band structure and projected DOS of bulk, cubic CsPbBr₃. The band gap occurs at the R point [$k = (1/2, 1/2, 1/2)$] and has an estimated gap of $E_g = 2.16$ eV. This agrees well with prior work suggesting $E_g = 2.39$ eV.^{47,48} The conduction band (CB) edge is largely Pb *p*-character whereas the valence band (VB) edge predominately arises from the overlap of Br *p*-orbitals. Dangling Br (Pb) bonds lead to defect states below (above) the VB maximum (CB minimum). Bulk CsPbBr₃ therefore possesses a surface defect-tolerant electronic structure similar to that seen in other lead-based semiconductors (e.g. PbSe).⁴⁹ Furthermore, a bulk Stokes shift of 20 meV³⁹ largely results from lattice-induced carrier stabilization and remains distinct from the size-dependent shifts observed in NCs. Details of these bulk CsPbBr₃ calculations can be found in the *SI* and in **Table S3**.

Given that the size-dependent electronic structure of CsPbBr₃ NCs remains relatively unexplored,¹⁹ our modeling efforts are premised on the idea that many geometrical models must be examined to consider the results robust. NC models with edge lengths of $l = 2.05$, 2.64, 3.23, 3.82, and 4.40 nm were therefore sampled across different morphologies and defects as summarized in **Table S4**. These calculations employ hybrid exchange functionals to suppress well known over-delocalization artifacts of generalized gradient approximations (GGA). Furthermore, they include spin-orbit^{50,51} and electron-hole exchange interactions to account for the existence of excitonic fine structure.^{24,52-54} In all cases, an adiabatic as-

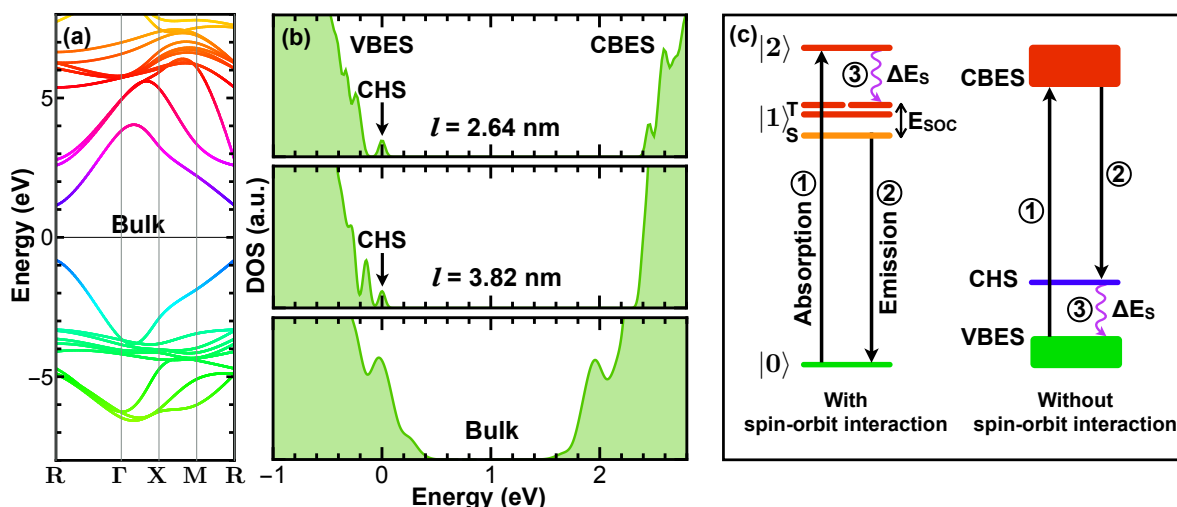


Figure 4: (a) Electronic band structure of bulk, cubic CsPbBr₃ calculated with the spin-orbit coupling interaction. (b) DOS for two NC sizes and the bulk material. The CHS shifts towards the VB edge as the NC size increases, eventually becoming indistinguishable from the bulk VB edge. (c) Model Jablonski diagrams show the fine structure resulting from SOC.

assumption—namely, that the electron-hole polaronic lattice relaxation is size-independent—is invoked.^{14,55}

Figure S10 shows resulting molecular orbitals (MOs) for the two lowest occupied VB states of $l = 2.64, 3.23, 3.82,$ and 4.40 nm NC models. In all cases, NC VB frontier states possess nodeless, cuboidal spatial distributions delocalized over the entire particle. This state, hereafter referred to as the confined hole state (CHS), exists in both cubic and orthorhombic models. Existence of the CHS is thus insensitive to NC crystal phase (**Figure S11**). Similar electronic structure has been observed in prior theoretical work conducted on CsPbBr₃ NCs, further supporting its existence.¹⁹ The most important result of these calculations is the fact that the CHS is delocalized over the entire NC. Consequently, it is spatially confined by the NC size and hence possesses size-dependent energies. This provides a basis for rationalizing observed size-dependent Stokes shifts, as discussed below.

These calculations simultaneously reveal that the next occupied NC level (260–70 meV above the CHS) closely resembles the bulk CsPbBr₃ VB maximum at the R point, hereafter referred to as the VB edge state (VBES). In contrast with the nodeless and diffuse nature of the CHS, the singly-noded VBES localizes near NC corners with a distinctive nodal plane

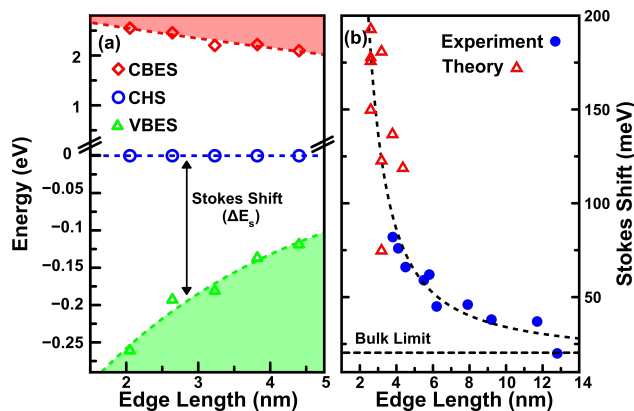


Figure 5: (a) Size-dependent NC CBES and VBES energies plotted relative to CHS energies, which are set to zero. State energies calculated at the Γ -point. Dashed lines are corresponding interpolation fits. (b) Experimental band edge excitation-derived ΔE_s values (closed blue circles) plotted against theoretical Stokes shifts (open red triangles).

cutting diagonally through the NC core. This is evidenced by an apparent phase change in calculated MOs (**Figure S10**). The calculations also show that the CB edge state (CBES) mirrors the bulk CB minimum at the R point. **Figure 4b** summarizes size-dependent CHS energies relative to complementary VBES and CBES levels for $l = 2.64$ nm and $l = 3.82$ nm NCs. Calculated bulk levels are shown for comparison purposes. A projected DOS for a $l = 2.64$ nm NC is provided in **Figure S12**.

CsPbBr₃ NC fine structure has simultaneously been investigated to assess its impact on observed Stokes shifts. This has been done by building a Breit-Pauli spin-orbit coupling (SOC) Hamiltonian^{50,51,56} with electron-hole exchange interactions between the four spin-adapted excitations linking the CHS and CBES. The four resulting fine-structure states are close in character to the three triplet and singlet states they are built from and are separated by 10 meV. This is consistent previously described fine structure for MAPbBr₃ and MAPbI₃.⁵⁷ **Figure 4c** (left) summarizes the energetic ordering of resulting fine structure states and depicts relevant absorption and emission transitions within a fine structure descriptor of CsPbBr₃ NCs. The calculations reveal that the magnitude of any spin-orbit induced fine structure splitting (E_{SOC}) ranges from 10.3 meV for a $l = 2.64$ nm NC to 0.13 meV for a $l = 3.82$ nm NC. Triplet/singlet fine structure splitting is therefore neg-

ligible for experimentally-relevant sizes (i.e. $\sim 4\text{--}13$ nm). We conclude that fine structure spin-orbit coupling/electron-hole exchange cannot explain observed size-dependent ΔE_s values. In what follows, we therefore do not invoke fine structure when rationalizing observed Stokes shifts. Note that this conclusion differs from the case of CdSe QDs where band edge fine structure was found to be responsible for intrinsic size-dependent “resonant” and “non-resonant” Stokes shifts.³¹ Details of the CsPbBr₃ fine structure modeling can be found in the *SI*.

At this point, NC band edge absorption in the model primarily occurs as a VBES \rightarrow CBES transition. This is followed by non-radiative relaxation of the photoexcited hole to the CHS whereupon emission occurs as a CBES \rightarrow CHS transition. A Stokes shift is therefore predicted with a magnitude that reflects the size-dependent energy difference between the CHS and VBES. Absorption/emission processes are summarized in **Figure 4c** (right). In support of this origin for the Stokes shift, the ratio of calculated VBES \rightarrow CBES and CHS \rightarrow CBES absorption strengths are substantial and differ 10- to 50-fold. This originates from differences in their underlying DOS as suggested by **Figure 4b**. As a result, the CHS \rightarrow CBES transition is relatively dark in absorption whereas the VBES \rightarrow CBES transition is bright. The generally small energetic separation of the CHS from the VBES along with significant VBES \rightarrow CBES line broadening, stemming from residual size distributions, is likely the reason why this transition is not seen in absorption. Further discussion and details of the absorption strength estimates can be found in the *SI*.

Figure 5a now illustrates calculated CHS/VBES energy differences for NCs with edge lengths between $l = 2.64$ nm and $l = 3.82$ nm. Apparent is an increase from 260 to 70 meV for models with $l \sim 2$ to 5 nm. Theoretical ΔE_s values are therefore size-dependent and of similar magnitude to experimental Stokes shifts. **Figure 5b** shows an explicit comparison of experimental and theoretical Stokes shifts and reveals that they are in quantitative agreement. The origin of a size-dependent Stokes shift in CsPbBr₃ NCs is therefore rationalized.

Remarkably, existence of the Stokes shift is robust with respect to crystal phase, NC

1
2
3 size, and defect type throughout the calculations (see **Figures S10, S11** and **Table S4**).
4
5 Size-dependent CHS→VBES energy differences exist in both cubic and orthorhombic models
6
7 and across different degrees of surface vacancies. An example is provided in the *SI*. Both
8
9 experimental and computational results therefore indicate that absorbing and emitting states
10
11 are distinct in CsPbBr₃ NCs. Of note is that the CHS is exclusive to NCs and does not
12
13 appear in the bulk. Furthermore, the calculations reveal that CsPbBr₃ NC CHS, VBES,
14
15 and CBES levels possess minimal cesium orbital character. Consequently, conclusions from
16
17 the current CsPbBr₃ NC model are likely applicable to other hybrid lead-halide perovskites.
18
19 Note that lattice relaxation in NCs does not explain observed size-dependent Stokes shifts
20
21 since calculated (upper limit) exciton binding energies are generally small and range from
22
23 $E_{bind} = 30$ to 60 meV. This corroborates a picture wherein diffuse electron-hole pairs weakly
24
25 interact with the nuclear lattice. Details of these calculations and a further discussion of
26
27 CsPbBr₃ NC exciton binding energies can be found in the *SI*.
28
29
30
31

32 Conclusion

33
34
35 In summary, we establish for the first time the origin of a size-dependent Stokes shift in
36
37 CsPbBr₃ NCs. These shifts range from 82 to 20 meV for particles with effective edge lengths
38
39 ranging from ~4 to 13 nm. We provide experimental proof to show that the shift is intrinsic
40
41 to the NC electronic structure. Using first-principles modeling, we identify an inherent,
42
43 size-dependent CHS level above the VBES, with the CHS dark in absorption and bright in
44
45 emission. Subsequently computed Stokes shifts from various geometric models quantitatively
46
47 agree with experimentally-measured values. The study therefore indicates that absorbing
48
49 and emitting states are distinct in CsPbBr₃ NCs and simultaneously rationalizes observed
50
51 Stokes shifts. At a broader level, since cesium orbitals do not significantly contribute to the
52
53 CHS, this state is likely a general feature of other perovskite NCs and can be tuned via NC
54
55 size to influence their response within photovoltaic or light-emitting applications.
56
57
58
59
60

Experimental

Synthesis and Purification of CsPbBr₃ NCs

Ensemble NC samples were synthesized with average edge lengths ranging from $l = 3.0\text{--}12.8$ nm using a hot injection method previously reported by Protesescu et al.⁷ Briefly, 0.18 mmol of PbBr₂ (99.999% trace metals basis, Sigma-Aldrich) and 5 mL of octadecene (ODE, 90% technical grade, Acros) were placed in a 10-mL three-neck flask and degassed at 120°C for 1 hour. The reaction vessel was back-filled with N₂. Then 1 mL of oleylamine (80-90% C-18 content, Acros) and 1 mL of oleic acid (90% technical grade, Sigma-Aldrich) were injected into it. The temperature was raised to 130–200°C in order to tune the size with higher (lower) temperatures favoring larger (smaller) NCs. Once the temperature stabilized, 1 mL of a Cs-oleate precursor solution (125 mM in ODE, prepared as described below) was injected. The reaction was then immediately quenched with an ice bath. The precipitate was separated by centrifuging the suspension at 7500 rpm for 10 minutes and was subsequently washed with a 4:1 mixture of toluene:acetone. Note that the addition too much acetone strips the surface ligands, causing them to aggregate. NCs were then dispersed in toluene and isolated using further centrifugation at 7500 rpm for 10 minutes. Recovered NCs were stored in toluene for further analysis. For smaller NC ensembles (in the range of $l \sim 3\text{--}6$ nm), reactions were scaled up 10-fold and the Cs-oleate precursor was injected at temperatures between 130° and 140°C.

Cs-oleate was synthesized according to a previous report.⁷ Briefly, 2.5 mmol of Cs₂CO₃ (99.9%, Sigma-Aldrich) was placed in a 100 mL three neck flask with 40 mL of ODE and 2.5 mL of oleic acid. The reaction mixture was degassed at 120°C for 1 hour and was then back-filled with N₂ and heated at 150°C for 6–8 hours. Cs-oleate exists as a precipitate at room temperature and must be heated to 100°C in order to dissolve it prior to injection.

Optical Measurements

Absorption Spectroscopy

Ensemble absorption spectra were obtained on a Cary 50 Bio UV-Visible spectrophotometer. Spectra were recorded under ambient condition in a fused silica cuvette using dilute solutions of CsPbBr₃ NCs in toluene. Optical densities were less than 0.3 in all cases.

Photoluminescence and Photoluminescence Excitation Spectroscopy

PL and PLE spectra were recorded under identical conditions as absorption spectra using a Jobin Yvon Fluorolog-3. In both PL and PLE measurements, excitation and emission slit widths were set to 2 nm and 1 nm, respectively. The integration time was 0.25 s with 1 nm increments. For PL measurements, the excitation wavelength was $\lambda_{exc} = 350$ nm. For band edge excitation measurements, λ_{exc} was set to the peak energy of each sample's band edge absorption. In PLE measurements, emission positions were taken on the red edge of each sample's band edge emission. PLE spectra were corrected for wavelength-dependent variations of the lamp intensity.

Photoluminescence Quantum Yield Measurements

PL QY measurements were performed according to a standardized procedure⁵⁸ with appropriate organic dyes [coumarin 6 (QY = 78%)⁵⁹ and coumarin 102 (QY = 74%)⁶⁰ for the green and blue regions of the spectrum respectively] dissolved in ethanol (100%, Sigma-Aldrich). The NC solvent was toluene. Optical densities were below 0.2 for both dye and NC samples.

Time-Correlated Single Photon Counting Time-Resolved Emission Spectroscopy

TCSPC-TRES measurements were obtained with a Horiba Jobin Yvon TCSPC Spectrometer with a NanoLED 371 nm excitation source. Time-resolved PL decays were measured over 120 nm in 2 nm increments. TCSPC-TRES spectra were constructed by taking slices of PL

1
2
3 decay series to obtain the spectrum at a given time after photoexcitation. Note that the
4 instrument response time is approximately 300 ps. Optical densities were below 0.2 in all
5 cases.
6
7
8
9

10 **Solvatochromism Measurements**

11
12 Ensemble samples for solvatochromism experiments were dried via vacuum and were re-
13 dispersed in hexanes and chloroform. Absorption and emission spectra were measured as
14 described above.
15
16
17
18
19

20 **Excitation Intensity-Dependent Emission Measurements**

21
22 NC ensembles for excitation intensity (I_{exc})-dependent emission measurements were
23 spin coated onto glass substrates (VWR micro cover glass, 25 mm). Emission intensities
24 were collected as a function of I_{exc} using a 405 nm continuous wave (CW) laser [Coherent,
25 Obis] focused onto samples using a high numerical aperture objective (0.65 NA, Nikon).
26 Excitation intensities ranged from 0.01-1.5 W/cm². The resulting emission was collected
27 with the same objective using a barrier filter (425LP, Chroma) to reject the laser. The
28 emission was subsequently detected with a single photon counting avalanche photodiode
29 (PerkinElmer, SPCM AQR-14).
30
31
32
33
34
35
36
37
38
39
40
41

42 **Powder X-Ray Diffraction Measurements**

43
44 Powder XRD measurements were acquired with a Bruker D8 Discover diffractometer with a
45 Cu K α source ($\lambda = 1.5418 \text{ \AA}$) in the Bragg-Brentano geometry. Measurements were recorded
46 from 10–60° 2θ with a step size of 0.01° and an integration time of 4 s per step.
47
48
49
50
51
52

53 **Transmission Electron Microscopy Measurements**

54
55 TEM images were acquired using both a FEI Titan 80-300 kV microscope with an acceler-
56 ating voltage of 300 kV and a JEOL 2011 microscope with an accelerating voltage of 200
57
58
59
60

1
2
3 kV. Samples were prepared by drop casting dilute NC solutions in toluene onto ultrathin
4
5 amorphous carbon substrates with copper supports (Ladd).
6
7

8 9 **Theoretical Modeling**

10
11 NC models were created starting with a $n \times n \times n$ supercell, where n is an integer repre-
12
13 senting the number of cubic unit cells. Due to the cubic nature of experimentally-observed
14
15 particles, as evidenced in this work and others,⁷ theoretical models are restricted to reflect
16
17 this morphology. For the cubic lattice, the (100), (010), and (001) directions are identical.
18
19 Each has two unique layers; one with only Cs and Br atoms and another with only Pb and
20
21 Br atoms. These are referred to as Cs-Br and Pb-Br layers, respectively. Orthorhombic
22
23 models were cut to supercells identical in stoichiometry to the cubic models, with the only
24
25 difference being the tilting of lead-bromide octahedra.
26
27

28
29 Only models terminated on all faces by the same layer, either a Cs-Br or a Pb-Br layer
30
31 were considered. Pure supercells have three faces terminated by a Cs-Br layer and three faces
32
33 terminated by a Pb-Br layer. To rectify this with our restriction that surface-terminating
34
35 layers be identical on all faces, each supercell model was extended by adding a Cs-Br (Pb-Br)
36
37 layer over the Pb-Br (Cs-Br) surface-terminating faces of the supercell.
38

39
40 To correctly simulate these NCs, geometrical models-of-interest must possess the fol-
41
42 lowing features: (1) charge neutrality, with near zero dipole moment and a stoichiometry
43
44 which closely follows the bulk molecular formula, (2) a crystalline structure observed in
45
46 experiments, and (3) surface defects known to this material. The first requirement puts
47
48 limitations on the surface-terminating layers for different-sized models unless defects deeper
49
50 than the surface layer are considered. For $n \times n \times n$ supercell models, an even integer n
51
52 requires that the surface be terminated with a Pb-Br layer. An odd integer n requires sur-
53
54 faces to be terminated with a Cs-Br layer. Minimal surface vacancy defects were made to
55
56 charge neutralize the models while maintaining a near zero dipole. Additional surface va-
57
58 cancy defects were considered to examine their effect on electronic structure. CsPbBr₃ NCs
59
60

1
2
3
4 have high surface defect tolerance, thus defects that break this high tolerance have large
5 formation energies.¹⁸ To validate that this defect tolerance fits with the Stokes shift model
6
7
8
9
10
11
12
13
14
15
16
17
18
19
20
21
22
23
24
25
26
27
28
29
30
31
32
33
34
35
36
37
38
39
40
41
42
43
44
45
46
47
48
49
50
51
52
53
54
55
56
57
58
59
60

have high surface defect tolerance, thus defects that break this high tolerance have large formation energies.¹⁸ To validate that this defect tolerance fits with the Stokes shift model posited in the study, a range of surface vacancy defects was explored. Models therefore considered varied placements as well as amounts of Cs, Pb, and Br surface vacancies.

Given the debate as to whether CsPbBr₃ NCs adopt cubic or orthorhombic phases, models of both phases were prepared. We explore models with two types of optimization: (1) only allowing surface atoms to relax, leaving the core atoms frozen, and (2) allowing the whole structure to undergo full geometry optimization. Doing so enabled us to rationalize whether there could be characteristics of either morphology or unique NC aspects which explained the Stokes shift.

NC calculations were done in CP2K 4.1⁶¹ with the Heyd-Scuseria-Ernzerhof (HSE) functional,⁶² a double- ζ quality basis set⁶³ and core potentials including relativistic effects.⁶⁴ Each model was calculated in a periodic cell with at least 15 Å of vacuum in each direction. Periodic calculations for the bulk cubic and orthorhombic structures were performed in the Quantum Espresso package⁶⁵ with the Perdew-Burke-Ernzerhof hybrid (PBE0) functional and a 500 eV plane-wave cutoff; scalar relativistic and spin-orbit interactions were included.

Acknowledgments

This work was supported by the Division of Materials Sciences and Engineering, Office of Basic Energy Sciences, U.S. Department of Energy under award DE-SC0014334. J.Z. acknowledges support from the Arthur J. Schmitt Fellowship Foundation. T. S. N.-B. acknowledges the support of the NSF Graduate Research Fellowship under grant DGE-131358 and the Patrick and Jana Eilers Graduate Student Fellowship for Energy Related Research. J. P. thanks the University of Notre Dame's College of Science and Department of Chemistry and Biochemistry, ND Energy and the Honeywell Corporation for generous start-up funding. S. R. thanks the University of Notre Dame Integrated Imaging Facility for financial support

1
2
3 of the work conducted on this project.
4
5
6

7 8 Author Information Notes

9
10
11 M.C.B and J.E.H. contributed equally to this work.
12
13

14 15 Associated Content

16
17
18 *Supporting Information Available.* NC sizing histogram, absorption- and emission-derived
19 NC sizing curves, NC PXRD data, excitation intensity-dependent emission data and dis-
20 cussion, table of PL quantum yields, table of relevant experimental absorption and emission
21 data, linear absorption fits, TCSPC-TRES data, solvatochromism data, band-edge excitation
22 emission and absorption spectra, convolution analysis of other ensemble NC sizes, discus-
23 sion of bulk electronic structure calculations, discussion of geometries and band structure
24 calculations, table of calculated bulk band gaps/lattice parameters, MOs for VBES/CHS of
25 different NC sizes, MOs for CHS of NC models with various crystal phases, projected DOS
26 for $l = 2.64$ nm NC model, discussion of spin-orbit coupling calculations, absorption strength
27 calculations discussion, table of NC model data, discussion of exciton binding energies. This
28 material is available free of charge via the Internet at <http://pubs.acs.org>.
29
30
31
32
33
34
35
36
37
38
39
40
41
42

43 44 References

- 45
46
47 (1) Snaith, H. J. *J. Phys. Chem. Lett.* **2013**, *4*, 3623–3630.
48
49 (2) Mitzi, D. B.; Feild, C.; Schlesinger, Z.; Laibowitz, R. *J. Solid State Chem.* **1995**, *114*,
50 159–163.
51
52
53
54 (3) Kagan, C.; Mitzi, D.; Dimitrakopoulos, C. *Science* **1999**, *286*, 945–947.
55
56
57
58
59
60

- 1
2
3
4
5
6
7
8
9
10
11
12
13
14
15
16
17
18
19
20
21
22
23
24
25
26
27
28
29
30
31
32
33
34
35
36
37
38
39
40
41
42
43
44
45
46
47
48
49
50
51
52
53
54
55
56
57
58
59
60
- (4) National Renewable Energy Labs Efficiency Chart (2017). <https://www.nrel.gov/pv/assets/images/efficiency-chart.png>, (accessed: May 6 2017).
- (5) Manser, J. S.; Christians, J. A.; Kamat, P. V. *Chem. Rev.* **2016**, *116*, 12956–13008.
- (6) Bai, S.; Yuan, Z.; Gao, F. *J. Mater. Chem. C* **2016**, *4*, 3898–3904.
- (7) Protesescu, L.; Yakunin, S.; Bodnarchuk, M. I.; Krieg, F.; Caputo, R.; Hendon, C. H.; Yang, R. X.; Walsh, A.; Kovalenko, M. V. *Nano Lett.* **2015**, *15*, 3692–3696.
- (8) Protesescu, L.; Yakunin, S.; Bodnarchuk, M.; Bertolotti, F.; Masciocchi, N.; Guagliardi, A.; Kovalenko, M. *J. Am. Chem. Soc.* **2016**, *10*, 2485–2490.
- (9) Zhang, F.; Zhong, H.; Chen, C.; Wu, X.-g.; Hu, X.; Huang, H.; Han, J.; Zou, B.; Dong, Y. *ACS Nano* **2015**, *9*, 4533–4542.
- (10) Zhang, D.; Eaton, S.; Yu, Y.; Dou, L.; Yang, P. *J. Am. Chem. Soc.* **2015**, *137*, 9230–9233.
- (11) Zhang, D.; Yu, Y.; Bekenstein, Y.; Wong, A. B.; Alivisatos, A. P.; Yang, P. *J. Am. Chem. Soc.* **2016**, *138*, 13155–13158.
- (12) Zhu, H.; Fu, Y.; Meng, F.; Wu, X.; Gong, Z.; Ding, Q.; Gustafsson, M. V.; Trinh, M. T.; Jin, S.; Zhu, X.-Y. *Nat. Mater.* **2015**, *14*, 636–642.
- (13) Fu, Y.; Meng, F.; Rowley, M.; Thompson, B.; Shearer, M.; Ma, D.; Hamers, R.; Wright, J.; Jin, S. *J. Am. Chem. Soc.* **2015**, *137*, 5810–5818.
- (14) Dou, L.; Wong, A. B.; Yu, Y.; Lai, M.; Kornienko, N.; Eaton, S. W.; Fu, A.; Bischak, C. G.; Ma, J.; Ding, T.; Ginsberg, N. S.; Wang, L.-W.; Alivisatos, A. P.; Yang, P. *Science* **2015**, *349*, 1518–1521.

- 1
2
3
4 (15) Akkerman, Q. A.; Motti, S. G.; Srimath Kandada, A. R.; Mosconi, E.; D’Innocenzo, V.;
5 Bertoni, G.; Marras, S.; Kamino, B. A.; Miranda, L.; De Angelis, F.; Petrozza, A.;
6 Prato, M.; Manna, L. *J. Am. Chem. Soc.* **2016**, *138*, 1010–1016.
7
8
9
10 (16) Bekenstein, Y.; Koscher, B. A.; Eaton, S. W.; Yang, P.; Alivisatos, A. P. *J. Am. Chem.*
11 *Soc.* **2015**, *137*, 16008–16011.
12
13
14
15 (17) Lang, L.; Yang, J.; Liu, H.; Xiang, H.; Gong, X. *Phys. Lett. A* **2014**, *378*, 290–293.
16
17
18 (18) Kang, J.; Wang, L.-W. *J. Phys. Chem. Lett.* **2017**, *8*, 489–493.
19
20
21 (19) ten Brinck, S.; Infante, I. *ACS Energy Lett.* **2016**, *1*, 1266–1272.
22
23
24 (20) Li, M.; Bhaumik, S.; Goh, T. W.; Kumar, M. S.; Yantara, N.; Grätzel, M.;
25 Mhaisalkar, S.; Mathews, N.; Sum, T. C. *Nat. Commun.* **2017**, *8*, 14350.
26
27
28 (21) Castañeda, J. A.; Nagamine, G.; Yassitepe, E.; Bonato, L. G.; Voznyy, O.; Hoogland, S.;
29 Nogueira, A. F.; Sargent, E. H.; Cruz, C. H. B.; Padilha, L. A. *ACS Nano* **2016**, *10*,
30 8603–8609.
31
32
33
34 (22) Makarov, N. S.; Guo, S.; Isaienko, O.; Liu, W.; Robel, I.; Klimov, V. I. *Nano Lett.*
35 **2016**, *16*, 2349–2362.
36
37
38
39 (23) Butkus, J.; Vashishtha, P.; Chen, K.; Gallaher, J. K.; Prasad, S. K.; Metin, D. Z.;
40 Laufersky, G.; Gaston, N.; Halpert, J. E.; Hodgkiss, J. M. *Chem. Mater.* **2017**, *29*,
41 3644–3652.
42
43
44
45 (24) Rainò, G.; Nedelcu, G.; Protesescu, L.; Bodnarchuk, M. I.; Kovalenko, M. V.;
46 Mahrt, R. F.; Stöferle, T. *ACS Nano* **2016**, *10*, 2485–2490.
47
48
49
50 (25) D’Innocenzo, V.; Srimath Kandada, A. R.; De Bastiani, M.; Gandini, M.; Petrozza, A.
51 *J. Am. Chem. Soc.* **2014**, *136*, 17730–17733.
52
53
54
55
56
57
58
59
60

- 1
2
3
4 (26) Makarov, N.; Guo, S.; Isaienko, O.; Liu, W.; Robel, I.; Klimov, V. *Nano Lett.* **2016**,
5 *16*, 2349–2362.
6
7
8 (27) Castaeda, J. A.; Nagamine, G.; Yassitepe, E.; Bonato, L. G.; Voznyy, O.; Hoogland, S.;
9 Nogueira, A. F.; Sargent, E. H.; Cruz, C. H. B.; Padilha, L. A. *ACS Nano* **2016**, *10*,
10 8603–8609.
11
12
13 (28) Park, Y.-S.; Guo, S.; Makarov, N. S.; Klimov, V. I. *ACS Nano* **2015**, *9*, 10386–10393.
14
15
16 (29) Yettapu, G. R.; Talukdar, D.; Sarkar, S.; Swarnkar, A.; Nag, A.; Ghosh, P.; Mandal, P.
17 *Nano Lett.* **2016**, *16*, 4838–4848.
18
19
20 (30) Efros, A.; Rosen, M.; Kuno, M.; Nirmal, M.; Norris, D.; Bawendi, M. *Phys. Rev. B*
21 **1996**, *54*, 4843–4856.
22
23
24 (31) Kuno, M.; Lee, J.; Dabbousi, B.; Mikulec, F.; Bawendi, M. *J. Chem. Phys.* **1997**, *106*,
25 9869–9882.
26
27
28 (32) Kuno, M. *J. Phys. Chem. Lett.* **2013**, *4*, 680–680.
29
30
31 (33) de Mello Donegá, C. *Phys. Rev. B* **2010**, *81*, 165303.
32
33
34 (34) Brennan, M. C.; Zinna, J.; Kuno, K. *ACS Energy Lett.* **2017**,
35
36
37 (35) Roo, J.; Ibáñez, M.; Geiregat, P.; Nedelcu, G.; Walravens, W.; Maes, J.; Martins, J.;
38 Driessche, I.; Kovalenko, M.; Hens, Z. *ACS Nano* **2016**, *10*, 2071–2081.
39
40
41 (36) Cottingham, P.; Brutchey, R. *Chem. Commun.* **2016**, *52*, 5246–5249.
42
43
44 (37) Yu, Y.; Zhang, D.; Kisielowski, C.; Dou, L.; Kornienko, N.; Bekenstein, Y.; Wong, A. B.;
45 Alivisatos, A. P.; Yang, P. *Nano Lett.* **2016**, *16*, 7530–7535.
46
47
48 (38) Bertolotti, F.; Protesescu, L.; Kovalenko, M. V.; Yakunin, S.; Cervellino, A.; Billinge, S.
49 J. L.; Terban, M. W.; Pedersen, J. S.; Masciocchi, N.; Guagliardi, A. *ACS Nano* **2017**,
50 *11*, 3819–3831.
51
52
53
54
55
56
57
58
59
60

- 1
2
3
4 (39) Rakita, Y.; Kedem, N.; Gupta, S.; Sadhanala, A.; Kalchenko, V.; Bhm, M. L.; Kul-
5 bak, M.; Friend, R. H.; Cahen, D.; Hodes, G. *Cryst. Growth Des.* **2016**, *16*, 5717–5725.
6
7
8 (40) Lide, D.; Haynes, W. *CRC Handbook of Chemistry and Physics*, 90th ed.; CRC Press:
9 Boca Raton, 2009.
10
11
12 (41) Muljarov, E.; Zhukov, E.; Dneprovskii, V.; Masumoto, Y. *Phys. Rev. B* **2000**, *62*, 7420.
13
14
15 (42) Giblin, J.; Kuno, M. *J. Phys. Chem. Lett.* **2010**, *1*, 3340–3348.
16
17
18 (43) De Mello Donegá, C. *Phys. Rev. B Condens. Matter* **2010**, *81*, 1–20.
19
20
21 (44) Stoumpos, C. C.; Malliakas, C. D.; Peters, J. A.; Liu, Z.; Sebastian, M.; Im, J.;
22 Chasapis, T. C.; Wibowo, A. C.; Chung, D. Y.; Freeman, A. J.; Wessels, B. W.;
23 Kanatzidis, M. G. *Cryst. Growth Des.* **2013**, *13*, 2722–2727.
24
25
26 (45) Sebastian, M.; Peters, J.; Stoumpos, C.; Im, J.; Kostina, S.; Liu, Z.; Kanatzidis, M.;
27 Freeman, A.; Wessels, B. *Phys. Rev. B* **2015**, *92*, 235210.
28
29
30 (46) Pushuk, I.; Pidzyrajlo, N. S.; Matsko, M. G. *Fiz. Tverd. Tela* **1981**, *23*, 2162–2165.
31
32
33 (47) Begum, R.; Parida, M. R.; Abdelhady, A. L.; Murali, B.; Alyami, N.; Ahmed, G. H.;
34 Hedhili, M. N.; Bakr, O. M.; Mohammed, O. F. *J. Am. Chem. Soc.* **2017**, *139*, 731–737.
35
36
37 (48) Zhang, X.; Lin, H.; Huang, H.; Reckmeier, C.; Zhang, Y.; Choy, W. C.; Rogach, A. L.
38 *Nano Lett.* **2016**, *16*, 1415–1420.
39
40
41 (49) Allan, G.; Delerue, C. *Phys. Rev. B* **2004**, *70*, 245321.
42
43
44 (50) Bethe, H. A.; Salpeter, E. E. *Quantum Mechanics of One- and Two-Electron Atoms*;
45 Springer, 1957.
46
47
48 (51) Shao, Y.; Gan, Z.; Epifanovsky, E.; Gilbert, A. T.; Wormit, M.; Kussmann, J.;
49 Lange, A. W.; Behn, A.; Deng, J.; Feng, X.; Ghosh, D.; Goldey, M.; Horn, P. R.; Jacob-
50 son, L. D.; Kaliman, I.; Khaliullin, R. Z.; Kuś, T.; Landau, A.; Liu, J.; Proynov, E. I.;
51
52
53
54
55
56
57
58
59
60

1
2
3 Rhee, Y. M.; Richard, R. M.; Rohrdanz, M. A.; Steele, R. P.; Sundstrom, E. J.;
4
5 III, H. L. W.; Zimmerman, P. M.; Zuev, D.; Albrecht, B.; Alguire, E.; Austin, B.;
6
7 Beran, G. J. O.; Bernard, Y. A.; Berquist, E.; Brandhorst, K.; Bravaya, K. B.;
8
9 Brown, S. T.; Casanova, D.; Chang, C.-M.; Chen, Y.; Chien, S. H.; Closser, K. D.;
10
11 Crittenden, D. L.; Diedenhofen, M.; Jr., R. A. D.; Do, H.; Dutoi, A. D.; Edgar, R. G.;
12
13 Fatehi, S.; Fusti-Molnar, L.; Ghysels, A.; Golubeva-Zadorozhnaya, A.; Gomes, J.;
14
15 Hanson-Heine, M. W.; Harbach, P. H.; Hauser, A. W.; Hohenstein, E. G.; Holden, Z. C.;
16
17 Jagau, T.-C.; Ji, H.; Kaduk, B.; Khistyayev, K.; Kim, J.; Kim, J.; King, R. A.; Klun-
18
19 zinger, P.; Kosenkov, D.; Kowalczyk, T.; Krauter, C. M.; Lao, K. U.; Laurent, A. D.;
20
21 Lawler, K. V.; Levchenko, S. V.; Lin, C. Y.; Liu, F.; Livshits, E.; Lochan, R. C.; Lu-
22
23 enser, A.; Manohar, P.; Manzer, S. F.; Mao, S.-P.; Mardirossian, N.; Marenich, A. V.;
24
25 Maurer, S. A.; Mayhall, N. J.; Neuscammann, E.; Oana, C. M.; Olivares-Amaya, R.;
26
27 O'Neill, D. P.; Parkhill, J. A.; Perrine, T. M.; Peverati, R.; Prociuk, A.; Rehn, D. R.;
28
29 Rosta, E.; Russ, N. J.; Sharada, S. M.; Sharma, S.; Small, D. W.; Sodt, A.; Stein, T.;
30
31 Stück, D.; Su, Y.-C.; Thom, A. J.; Tsuchimochi, T.; Vanovschi, V.; Vogt, L.; Vy-
32
33 drov, O.; Wang, T.; Watson, M. A.; Wenzel, J.; White, A.; Williams, C. F.; Yang, J.;
34
35 Yeganeh, S.; Yost, S. R.; You, Z.-Q.; Zhang, I. Y.; Zhang, X.; Zhao, Y.; Brooks, B. R.;
36
37 Chan, G. K.; Chipman, D. M.; Cramer, C. J.; III, W. A. G.; Gordon, M. S.;
38
39 Hehre, W. J.; Klamt, A.; III, H. F. S.; Schmidt, M. W.; Sherrill, C. D.; Truh-
40
41 lar, D. G.; Warshel, A.; Xu, X.; Aspuru-Guzik, A.; Baer, R.; Bell, A. T.; Besley, N. A.;
42
43 Chai, J.-D.; Dreuw, A.; Dunietz, B. D.; Furlani, T. R.; Gwaltney, S. R.; Hsu, C.-P.;
44
45 Jung, Y.; Kong, J.; Lambrecht, D. S.; Liang, W.; Ochsenfeld, C.; Rassolov, V. A.;
46
47 Slipchenko, L. V.; Subotnik, J. E.; Voorhis, T. V.; Herbert, J. M.; Krylov, A. I.;
48
49 Gill, P. M.; Head-Gordon, M. *Mol. Phys.* **2015**, *113*, 184–215.

- 50
51
52
53 (52) Yin, C.; Chen, L.; Song, N.; Lv, Y.; Hu, F.; Sun, C.; William, W. Y.; Zhang, C.;
54
55 Wang, X.; Zhang, Y. *Phys. Rev. Lett.* **2017**, *119*, 026401.

- 1
2
3
4 (53) Tanaka, K.; Takahashi, T.; Ban, T.; Kondo, T.; Uchida, K.; Miura, N. *Solid State*
5 *Commun.* **2003**, *127*, 619–623.
6
7
8
9 (54) Fu, M.; Tamarat, P.; Huang, H.; Even, J.; Rogach, A. L.; Lounis, B. *Nano Lett.* **2017**,
10 *17*, 2895–2901.
11
12
13 (55) Emin, D. *Phys. Rev. B* **1971**, *4*, 3639.
14
15
16 (56) Sayfutyarova, E. R.; Chan, G. K.-L. *J. Chem. Phys.* **2016**, *144*, 234301.
17
18
19 (57) Tanaka, K.; Takahashi, T.; Ban, T.; Kondo, T.; Uchida, K.; Miura, N. *Solid State*
20 *Commun.* **2003**, *127*, 619–623.
21
22
23
24 (58) Grabolle, M.; Spieles, M.; Lesnyak, V.; Gaponik, N.; Eychmüller, A.; Resch-Genger, U.
25 *Anal. Chem.* **2009**, *81*, 6285–6294.
26
27
28
29 (59) Reynolds, G. A.; Drexhage, K. H. *Opt. Commun.* **1975**, *13*, 222–225.
30
31
32 (60) Jones, G.; Jackson, W. R.; Halpern, A. M. *Chem. Phys. Lett.* **1980**, *72*, 391–395.
33
34
35 (61) (a) Bortnik, U.; VandeVondele, J.; Weber, V.; Hutter, J. *Parallel Comput.* **2014**, *40*,
36 4758; (b) Hutter, J.; Iannuzzi, M.; Schiffmann, F.; VandeVondele, J. *Wiley Interdiscip.*
37 *Rev. Comput. Mol. Sci.* **2014**, *4*, 15–25; (c) Guidon, M.; Hutter, J.; VandeVondele, J.
38 *J. Chem. Theory Comput.* **2010**, *6*, 2348–2364; (d) Guidon, M.; Hutter, J.; VandeVon-
39 dele, J. *J. Chem. Theory Comput.* **2009**, *5*, 3010–3021; (e) Genovese, L.; Deutsch, T.;
40 Goedecker, S. *J. Chem. Phys.* **2007**, *127*, 054704; (f) Genovese, L.; Deutsch, T.;
41 Neelov, A.; Goedecker, S.; Beylkin, G. *J. Chem. Phys.* **2006**, *125*, 074105; (g) Van-
42 deVondele, J.; Krack, M.; Mohamed, F.; Parrinello, M.; Chassaing, T.; Hutter, J.
43 *Comput. Phys. Commun.* **2005**, *167*, 103 – 128; (h) Frigo, M.; Johnson, S. G. *Proc.*
44 *IEEE* **2005**, *93*, 216–231; (i) VandeVondele, J.; Hutter, J. *J. Chem. Phys.* **2003**, *118*,
45 4365–4369.
46
47
48
49
50
51
52
53
54
55
56
57
58 (62) Heyd, J.; Scuseria, G. E. *J. Chem. Phys.* **2004**, *120*, 7274–7280.
59
60

- 1
2
3
4 (63) VandeVondele, J.; Hutter, J. *J. Chem. Phys.* **2007**, *127*, 114105.
5
6
7 (64) Krack, M. *Theor. Chem. Acc.* **2005**, *114*, 145–152.
8
9 (65) Giannozzi, P.; Baroni, S.; Bonini, N.; Calandra, M.; Car, R.; Cavazzoni, C.; Ceresoli, D.;
10 Chiarotti, G. L.; Cococcioni, M.; Dabo, I.; Dal Corso, A.; de Gironcoli, S.; Fabris, S.;
11 Fratesi, G.; Gebauer, R.; Gerstmann, U.; Gougoussis, C.; Kokalj, A.; Lazzeri, M.;
12 Martin-Samos, L.; Marzari, N.; Mauri, F.; Mazzarello, R.; Paolini, S.; Pasquarello, A.;
13 Paulatto, L.; Sbraccia, C.; Scandolo, S.; Sclauzero, G.; Seitsonen, A. P.; Smogunov, A.;
14 Umari, P.; Wentzcovitch, R. M. *J. Phys. Condens. Matter* **2009**, *21*, 395502.
15
16
17
18
19
20
21
22
23
24
25
26
27
28
29
30
31
32
33
34
35
36
37
38
39
40
41
42
43
44
45
46
47
48
49
50
51
52
53
54
55
56
57
58
59
60

Graphical TOC Entry

